THERMAL STABILITY ASSESSMENT OF STANDARD & REDUCED Ni(Co)-Pd-Au METALLIZATION THICKNESS ON Cu-Mo70Cu-Cu HEATSPREADERS THROUGH SURFACE CHARACTERIZATION

Marty Lorgino D. Pulutan, Jerlyn B. Bermudez, Bongbong A. Mendoza

Backend Technologies
Ampleon Philippines, Inc., Light Industry & Science Park I, Brgy. Diezmo, Cabuyao City, Laguna
marty.lorgino.pulutan@ampleon.com

ABSTRACT

The thermal stability of standard and reduced Ni(Co)-Pd-Au metallization thickness on Cu-Mo70Cu-Cu heatspreaders were assessed through surface characterization to determine the optimum feasible thickness reduction in Au layer to deliver significant cost down without affecting the material reliability and performance. Three different plating thickness configurations were used and compared in response of surface morphology, surface composition, surface topography and plating thickness measured at every heat process step. Results showed that both plating configurations with reduced thickness have comparable thermal stability based on non-evolving surface morphology and surface topography. Evidence of Pd and Ni diffusion is observed on all three heatspreader types with percent atomic concentration exhibiting strong collinearity with Au thickness. Au layer depletion is observed on higher magnification SEM imaging but does not reflect on plating thickness measurement potentially due to non-uniform Au diffusion with Ag. Overall, the workable Au plating thickness range is 0.1 to 0.3µm minimum based on thermal stability exhibited by Reduced Version 2 (RV2) and Standard (STD) heatspreaders in response of surface characterization after series of high temperature exposure and aging.

1. 0 INTRODUCTION

Wide Bandgap (WBG) semiconductors have become increasingly popular in recent decades, enabling devices to function at greater power and higher frequencies, resulting in enhanced efficiency and power density. WBG semiconductors like GaN and SiC enable manufacturers to expand their product range and portfolio in the market, particularly in power electronics, where traditional Si semiconductors have reached their operational limits. The requirements become more complex with innovation which necessitates manufacturers for further miniaturization on the purpose of delivering dense functionality. The inverse trend of device dimensions with increasing power application generates tremendous heat which should be effectively dissipated from the integrated circuit device down to heatsink and is then spread throughout the board and on the entire system without reliability failure.

Cu heatspreaders are widely used as conventional substrates for Si devices but are deemed less compatible with GaN and SiC due to high Coefficient of Thermal Expansion (CTE) mismatch. Alternatively, a composite material comprised of Mo70-Cu alloy core sandwiched betweed two Cu clad layers known as Cu-CuMo-Cu provides varying CTE along x and y axis which minimizes the thermomechanical stress along joints [1]. The composite flanges are coated with Electroless Nickel Immersion Gold (ENIG), ensuring a robust adhesion with the die attach material which is slowly shifting from eutectic Au alloys to Ag sintering. To produce more commercially competitive package assembly materials, thickness of Au layer is further reduced significantly to offset the increase in raw Au cost. However, the Au thickness directly impacts the intermetallic or sintered joint as the Au interdiffuses into the die attach material to form connection for heat dissipation. The drive for further reducing Au thickness adds up to the challenge of forming a uniform sintered interface due to the difference in diffusion mechanism with Ag. The Ag atoms diffuse into Au matrix through grain boundaries which are prominent for thin Au layer thicknesses and thus forms a fragile Ag-Au solid solution layer [2]. Moreover, thin Au layer triggers diffusion of Ni atoms on top surface forming NiO forming weak layer interface with the die attach material [3]. A Pd layer is then inserted between the Ni and Au layer which acts as diffusion barrier suppressing such phenomenon [4].

2. 0 REVIEW OF RELATED WORK

Ni-Pd-Au plating has long been the standard surface finish favored by power industries due to its compatibility with Au wirebonding and lower risk of Ag migration [5]. Nevertheless, rising costs of Au raw materials have prompted manufacturers to investigate thinner Au plating with the assumption that material performance will remain uncompromised. Consequently, the main concerns associated with reducing the thickness of the Au layer are the potential dissolution and interdiffusion of Au with the die attach material, as well as the surface diffusion of Ni resulting in

NiO formation. Several studies have reported to observe such phenomenon especially with sintered Ag die attach and during high and prolonged temperature exposures. Paknejad et. al [6] reported that the Au layer is observed to dissolve within the sintered structure of Ag when thermally aged at 300°C for 500 hours where they claimed that Au rapidly interdiffuses with Ag forming Void-Free Layer on top of Au plating layer. Portions of the Au layers are observed to be completely depleted exposing underneath layers which provided pathway for ease of diffusion. Such results agree with the findings from the study of Yu et al. where they observed a dense and low porosity sintered Ag structure on top of Au surface. Elemental analysis of the cross-sectioned samples revealed presence of both Ni and Au within the dense sintered Ag structure forming an adjacent weak high porosity zone where early cohesive failure occur [5]. It was asserted that a Au thickness of approximately 0.07µm is inadequate to supply sufficient Au atoms for interdiffusion with Ag during thermal aging, resulting in depletion zones on the metallization thus exposing the underlying layer. This depletion also led to the formation of nickel oxide (NiO), contributing to cohesive fractures in the die attach [98].

In this study, the thermal stability of different heatspreader plating configuration was assessed through surface characterization to determine the optimal Au plating thickness without indication of Ni diffusion, Au dissolution and depletion leading to delamination.

3.0 METHODOLOGY

The 3-layered composite laminate heatspreader with Cu-CuMo-Cu stacking were obtained from local supplier plated with three different thickness configurations as shown in diagram below:

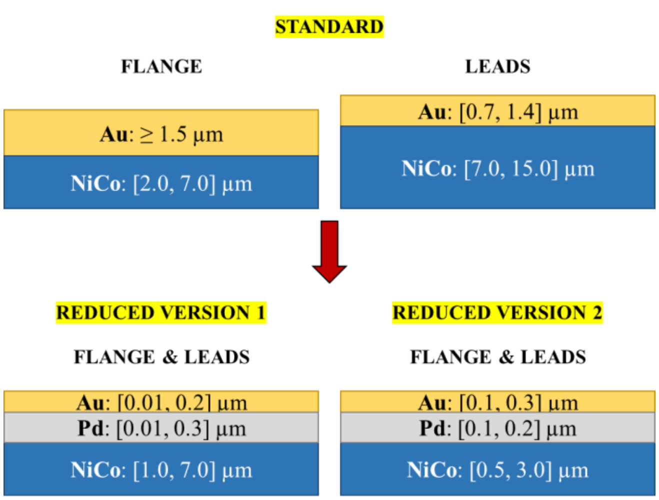

Fig. 1. Standard and reduced plating configurations of Cu-CuMo-Cu heatspreaders. Images were not drawn to scale.

The configurations specifically the thicknesses, were discussed and proposed with the supplier based on current capability and cost reduction. The standard (STD) heatspreader has different thickness on flange and leads as required by the test designers to minimize risk of lead heating. For reduced version 1 (RV1), Au thickness is significantly reduced to almost 60 folds than standard to lower down the cost but a Pd layer was inserted in between the Ni(Co) and Au, as barrier to prevent Ni diffusion. On the other hand, the Au thickness is marginally increased in reduced version 2 (RV2) configuration by ten folds compared to RV1 to lower the risk of Au depletion on surface. Comparison between RV1 and RV2 would distinguish optimum Au thickness range in terms of adhesion and cost.

From each of heatspreader type, 30 units were obtained and subjected to series of high temperature exposure corresponding to the assembly process flow of the package carrier and until High Temperature Storage Limit (HTSL) to assess the reliability against prolonged heat exposure. The utilized temperature and exposure time per process step is shown in Fig. 2.

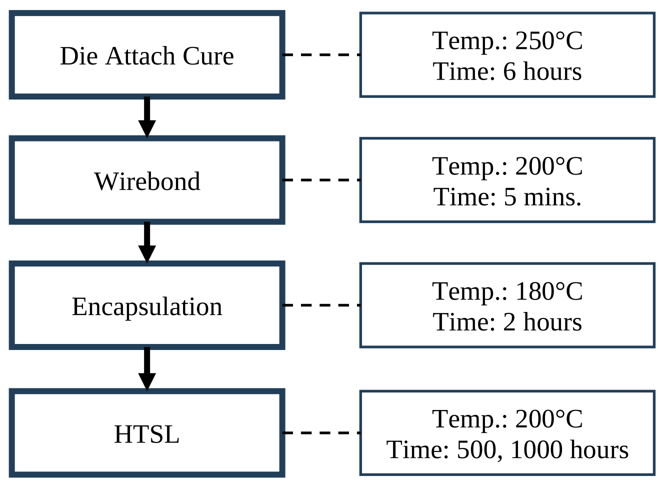

Fig. 2. Heat exposure process flow and the corresponding temperature and time condition per step.

From time zero up to HTSL 1000 hours at every process step, thermal stability of each header type was assessed through several material responses and metric specifically visual inspection through high magnification scope at 10x magnification, surface topography using Contour GT Bruker 3D Optical Profiler, surface morphology and composition using SEM-EDX Phenom XL, surface plating thickness evolution using X-ray Fluoresence (XRF) and surface wettability using goniometer through sessile drop technique. Surface topographical changes were investigated using two parameters – average roughness (R_a), roughness range (R_z) and surface warpage (W_t) whereas surface diffusion was examined using EDX at 5kV accelerating voltage using the mentioned equipment. Each measurement was recorded and mapped against each readpoint as time-series plot.

4.0 RESULTS AND DISCUSSION

4.1 Visual Changes of Heatspreaders With Varying Au Thicknesses

All 30 units per heatspreader type were subjected to visual inspection using high magnification scope at 10x to check the surface changes after High Temperature Storage Test (HTSL) at 200°C after 1000 hours.

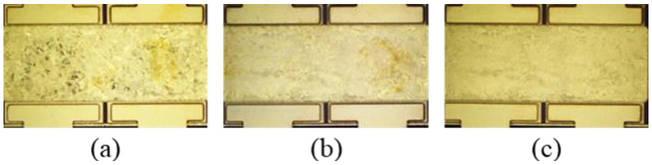

Fig. 3. Low Magnification Scope Images of (a) Standard, (b) Reduced Version 1 and (c) Reduced Version 2 Taken After 1000 Hours HTSL 200°C.

At time zero, as-received RV1 heatspreaders showed less visible Au grains than STD ones which show distinct Au grains possessing polycrystalline structure. The brazing material CuAg shows flow marks especially on leads while etching and burnt marks are prominent on both RV1 and RV2 which are not observed on STD due to reduced Ni thickness. RV1 and RV2 samples are less lustrous than STD and the color has further faded after exposure to series of high temperature, possibly indicating Ni and/or Pd diffusion which could be verified through EDX. RV1 and RV2 have no significant differences in terms of surface appearance regardless of their Au layer thickness difference.

4.2 Ni and Pd Diffusion of Heatspreaders With Varying Au Thicknesses

The elemental composition on the surface of each heatspreader type was examined using EDX at 5kV to minimize the penetration depth and target detection at surface level only.

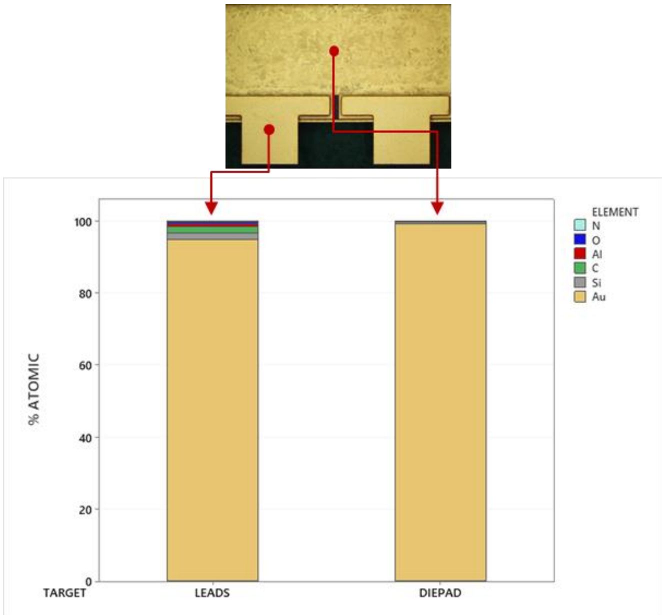

Fig. 4. Detected Elements and Their Corresponding % Atomic Concentration Measured at the Surface Level of RV1 at Time-Zero As-Received Condition.

EDX spectra for all heatspreader types showed absence of Pd or Ni at time-zero. However, Pd started to to diffuse after die attach cure heat exposure with average of 3% for RV1, 2.5% for RV2 and 1% for STD. Oxides are also detected possibly attributed to PdO diffused and formed on top of the flange surface. The test was repeated after HTSL 1000 hours to check for any further diffusion on the surface and possible oxide formations.

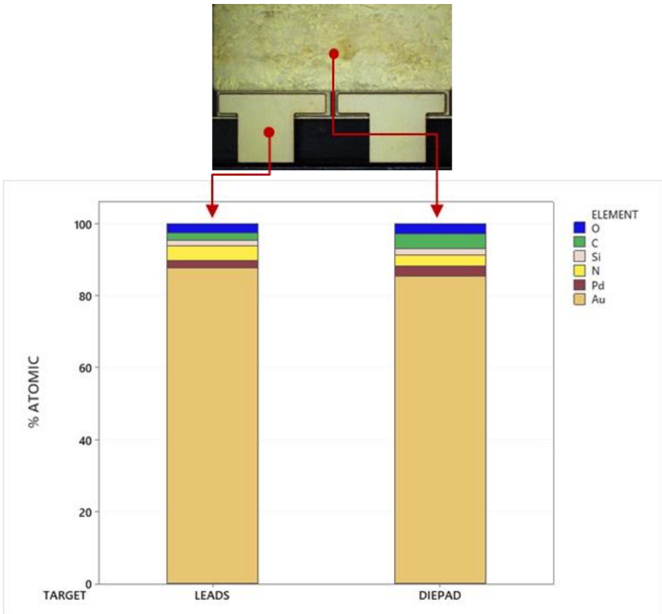

Fig. 5. Detected Elements and Their Corresponding % Atomic Concentration Measured at the Surface Level of RV1 Post HTSL 1000 Hours.

Post HTSL 1000 hours showed significant traces of elements not detected during preceding readpoints particularly Ni along with increase concentrations of O_2 indicating formation of NiO on top surface layer. The RV2 samples also showed traces of Ni but significantly lower at an average of 2.2% against RV1 which exhibited around 5.0% atomic concentration. The STD types have also shown traces of Ni but only up to 0.9% and O_2 at around 1.0%. Moreover, Pd was observed to be stagnant at the detected amount at post die attach cure and until HTSL 1000 indicating that Pd diffusion was either halted or has attained maximum diffusion at that temperature range regardless of multiple or prolonged exposures. The coefficient of determination between Au thickness and atomic concentration of Ni is obtained to be around 0.87 indicating strong correlation between the two variables. The correlation suggests that the thin Au allows Ni atoms to diffuse on top surface and that Pd layer is not sufficient to prevent the Ni atoms to traverse going to top surface where it reacts with native O_2 thus forming NiO.

4.3 Surface Morphology Alteration Across Heat Exposures

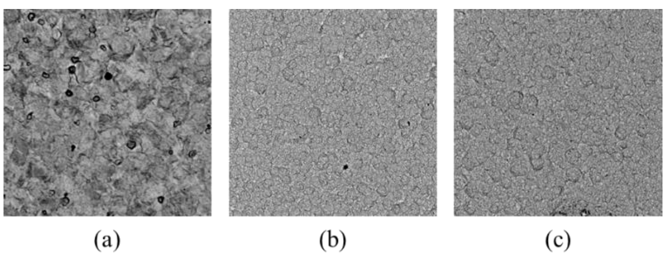

Fig. 6. Surface Morphology of (a) STD, (b) RV1, and (c) RV2 After HTSL 1000 Hours.

SEM images of STD samples exhibited visible large grains of Au accompanied with coarse texture emphasizing the grain boundaries from adjacent grains. Dislocations on some scanned areas on the flange are present possibly obtained during plating heat bath exposure and rapid cooling. However, scanning the entire area of both flange and leads showed non-uniformity in terms of grain structure and sizes, as some regions possess deep dents and sharp peaks and some parts show plateau and valleys. On the other hand, no significant distinction between RV1 and RV2 in terms of surface morphological characteristics. Both have displayed uniform distribution of crater-like structures which could denote higher surface roughness. Overall, the morphological structures on all heatspreader types have not evolved during heat exposures.

4.4 Surface Roughness Alteration Across Heat Exposures

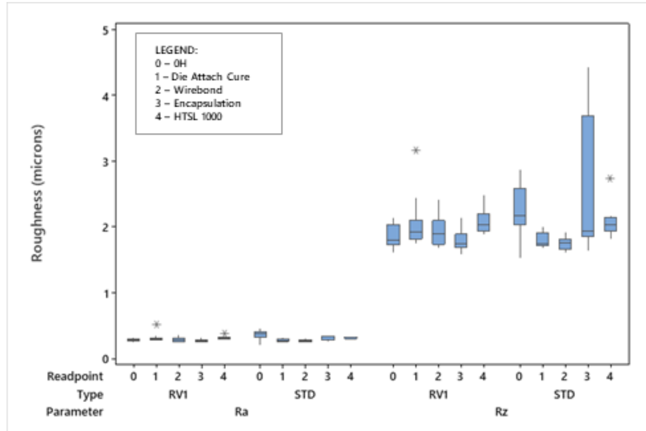

Fig. 7. Average Roughness (R_a) and Roughness Range (R_z) of STD and RV1 Heatspreaders Measured at Every Readpoint. Only RV1 is included in the plot for simplicity of comparison as RV1 and RV2 have not shown significant difference in roughness measurements.

Both R_a and R_z were measured through line scan of each of the 30 units per heatspreader type and the averages per readpoint per type is presented in Fig. 7. Using Repeated Measures ANOVA and pairwise comparison posthoc tests, no significant difference in terms of both roughness parameters between RV1 and RV2 is observed which indicates that 10-fold higher of Au thickness did not contribute to overall surface roughness of RV2. At time-zero, STD appear to be rougher than RV1 and RV2 but have significantly decreased after series of heat exposures potentially due to Pd and Ni diffusion on top surface which evens out the deeper trenches and crevices on the surface as detected in SEM imaging. The R_z of STD types has shown higher variance indicating presence of deep trenches and high peaks on the surface against RV1 and RV2 which are both relatively consistent in roughness measurement. The diffused Pd and Ni together with oxides formed however, did not manifest in terms of surface roughness as the diffused atoms may have not disturbed the intrinsic surface topography due to insignificant thickness. The warpage of the heatspreaders were also measured and were observed to be within 3.2. to 4.6 µm which are all well below the acceptable value in assembly and did not increase with heat exposures.

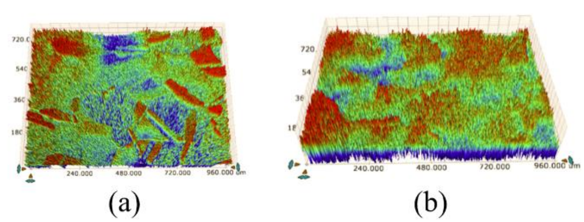

Fig. 8. 3D Optical Surface Profile of (a) STD and (b) RV1. Only RV1 is included in the illustration for simplicity of comparison as RV1 and RV2 have not shown significant difference in roughness measurements.

As shown in Fig. 8, STD samples exhibit visible elevated grains with sharp structures and deeper trenches and crevices whereas RV1 and RV2 have less deep valleys and finer surfaces which agrees with findings in SEM imaging. The surface did not exhibit any apparent topographical change after series of heat exposure which indicates thermal stability of roughness and warpage.

4.5 Surface Wettability Changes Across Heat Exposures

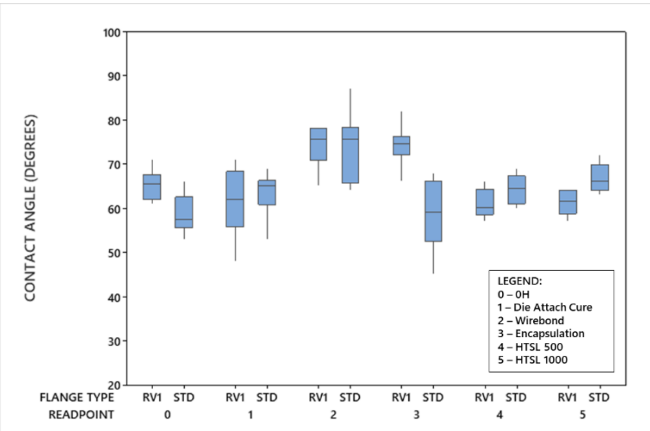

Fig. 9. Contact Angle of RV1 and RV2 Heatspreaders Measured at Every Readpoint. Only RV1 is included in the plot for simplicity of comparison as RV1 and RV2 have not shown significant difference in wettability measurements.

Using same statistical tests done on roughness data, RV1 and RV2 have not shown any significant difference in contact angle at every readpoint. The wettability of RV1 and STD types have shown observable difference, but no particular trend can be deduced from the data which implies that the wettability of the heatspreaders is not affected by heat exposures but possibly by other factors such as cleanliness of surface which directly impacts the surface energy. Nevertheless, the reduced plating thickness configurations are acceptable in terms of wettability response.

4.6 Plating Layer Thickness Evolution Across Heat Exposures

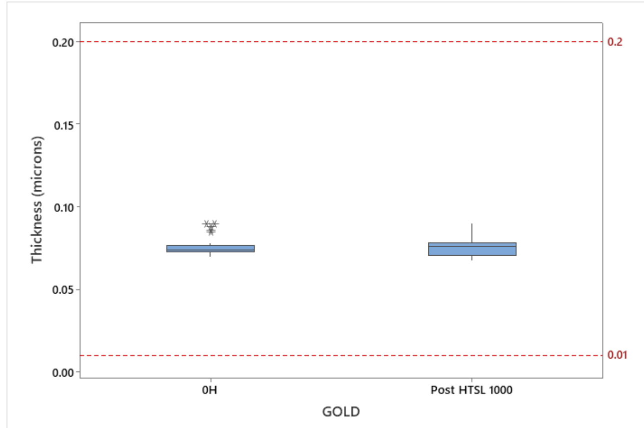

Fig. 10. Au Plating Layer Thickness of RV1 Measured at Time-Zero and After HTSL 1000 Hours.

The potential depletion and thinning of each plating layer were assessed using XRF and is presented in Fig. 10. The Ni, Pd and Au were all observed to be within thickness specifications during as-received conditions and did not decrease until HTSL 1000 hours exposure which suggests that the diffusion of Ni and Pd does not significantly reduce the thickness of their respective originating layer. However, the potential diffusion and depletion of thin Au layer cannot be assessed by measuring the bare heatspreaders alone and thus needs to be done with bonded Si dies and die attach.

4.6 Au Dissolution and Interdiffusion With Ag During Thermal Aging

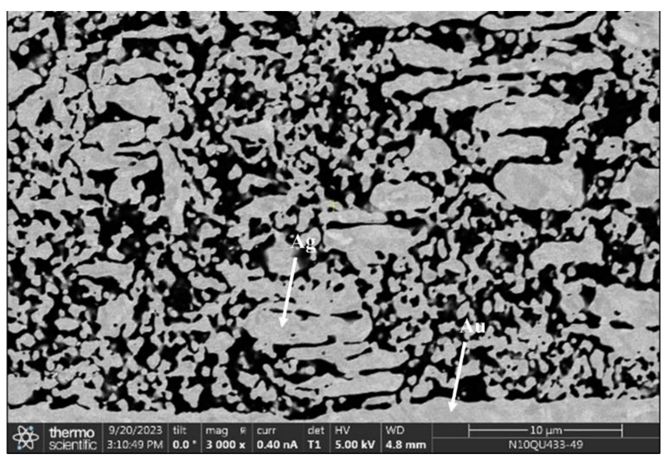

Fig. 11. SEM Image of Cross-Sectioned RV1 Samples at Time-Zero and After Encapsulation.

Higher SEM magnification on cross-sectioned RV1 samples revealed migration of Ag towards Au surface creating bonding and necking which is presumed to be penultimate stage to formation of VFL sintered Ag. Inspecting the Au layer showed thinner plating areas with almost exposed Pd and Ni(Co) layer indicating rapid dissolution and diffusion of Au atoms to adjacent low porosity sintered Ag layer. The higher Au thickness RV2 and STD heatspreaders have exhibited similar occurrences but Au plating layer is still intact and discernible against the VFL sintered layer. Such findings suggest that the potential workable thickness range for Au to prevent depletion zones and NiO formation is within 0.1 to 0.3μm minimum.

4.6 Reliability of Heatspreaders With Varying Au Thicknesses

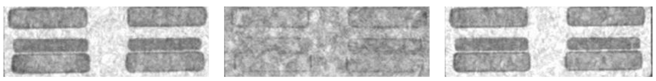

(a) (b) (c)

Fig. 12. Sampled SAM Images of (a) STD, (b) RV1, and (c) RV2 Post HTSL 1000 hours.

The SAM C-mode images verified the complete detachment of the sintered Ag structure from the pad surface of RV1 samples, whereas intact interfaces were observed for both STD and RV2. The possible diffusion of Au atoms and their interdiffusion with sintered Ag resulted in the depletion of the 0.01 to 0.2μm Au top layer, exposing Pd and facilitating the diffusion of detrimental Ni atoms. The insufficient presence of Au atoms led to the formation of a Void-Free Layer (VFL) of sintered Ag on top of an almost-depleted Au layer, creating two weak interfaces – a porous zone atop the VFL and the VFL-to-plating interface, which is highly fragile and brittle due to the presence of NiO, eventually leading to complete delamination.

5.0 CONCLUSION

The thermal stability of standard and reduced plating thicknesses was successfully evaluated in terms of surface morphology, surface composition, surface topography and plating thickness evolution measured at every heat process step exposure and post thermal aging. The STD heatspreaders exhibited superlative performance among the evaluated types based on very low Ni, Pd and O_2 percent atomic concentration but shows a distinct surface morphology that is different with RV1 and RV2 types. On the other hand, RV1 and RV2 have shown comparable material responses at every heat exposure but apparent depletion zones were observed on RV1 during thermal aging indicating rapid migration and dissolution of Au on sintered Ag matrix exposing underneath plating layers making it susceptible to diffusion and oxide formation. The workable Au plating thickness range is deduced to be within 0.1 to 0.3μm minimum to prevent formation of high porosity zones adjacent to VFL which causes early cohesive fracture. Further investigation during thermal aging is recommended such as conducting shear strength tests and inspecting failure and fragility zones.

6.0 RECOMMENDATIONS

The researchers recommend to correlate varying Au thickness with the microstructural evolution of die attach material particularly Ag sinter during thermal ageing to determine the optimal thickness that could survive long exposure to high temperature. Moreover, the use of other heatspreader laminate and other type of header or leadframe with varying plating thickness is suggested to confirm validity of results across different substrate composition. Lastly, it is noteworthy to check the effect of varying Au thickness and plating reconfiguration on the test response and overall test performance of the product.

7.0 ACKNOWLEDGMENT

The authors wish to extend their deepest appreciation to the engineers and technicians at the Backend Technologies Competence Center for their assistance in conducting the experiments, to Failure Analysis & Reliability Department, for the execution and provision of necessary tools, tests and support in the experiment, and to the management team of Ampleon Phils. Inc. for their support, which was instrumental in facilitating this research.

8.0 REFERENCES

1. A. Ali, ***Appl. Therm. Eng***., *181*, **2020**, 115984.

2. T. Fan, et al, ***J. Alloys Compd.***, *731*, **2018**, 1280-1287.

3. J. Yoon, et al., ***J. Electron. Mater.***, *40(9)*, **2011**, 1950-1955.

4. F. Yu, et al., ***IEEE Trans. Power Electron.***, *32(9)*, **2017**, 7083-7095.

5. S. A. Paknejad, et al, ***J. Alloys Compd.***, *617*, **2014**, 994-1001.

6. H. Zhang, et al, ***J. Alloys Compd.***, *774*, **2019**, 487-494.

9.0 ABOUT THE AUTHORS

Marty Lorgino D. Pulutan received the B. S. degree in Applied Physics specializing in Materials Physics from University of the Philippines, Los Baños in 2017 and currently pursuing M. S. degree in Materials Science and Engineering by Research in Mapua University. He has published a total of 10 papers in peer-reviewed journals and international conference proceedings. He is currently a Senior Materials Development Engineer under Back End Technologies Department in Ampleon Philippines, Inc.

Jerlyn B. Bermudez received the B. S. degree in Electronics

& Communications Engineering from Technological University of the Philippines, Taguig in 2010. She is currently a Senior Diebond Engineer under Back End Technologies Department in Ampleon Philippines, Inc.

Bongbong A. Mendoza received the B. S. degree in Electronics & Communications Engineering from Saint Louis University, Baguio City in 1992. He is currently a Principal Engineer – Project Management under Back End Technologies Department in Ampleon Philippines, Inc.